Interfacial structures and mechanical response of highly viscous polymer melt on solid surfaces investigated by atomic force microscopy

*Yuto Nishiwaki, Yuya Yamada, Toru Utsunomiya, Hiroyuki Sugimura, and Takashi Ichii**

Department of Materials Science and Engineering, Kyoto University, Yoshida Honmachi, Sakyo, Kyoto, 606-8501, Japan.

ABSTRACT

The interfacial structures and mechanical response of the highly viscous poly(dimethylsiloxane) (PDMS, 9750 mPa・s, M_n ~ 59000) on solid surfaces were investigated by frequency-modulation atomic force microscopy (FM-AFM) using a quartz tuning fork sensor. A layered density distribution on a PDMS/mica interface was visualized on a 29 h-settling sample by two-dimensional frequency shift (Δf) mapping, and the result exhibited that the layered structure was metastable. It was also found that the damping coefficient of tip vibration ($\Delta\gamma$) increased in the region of ~1 nm from the solid surface, which suggests the limited mobility of the liquid molecules closest to the solids. After settling for more extended time or heating the sample, the layered density distribution was suppressed, and the conservative repulsive force near the solid surface in 2-3 nm were observed over longer distances by settling for a more extended time or heating. The suppression of the layered density distribution showed the similar temperature dependence with the bulk viscoelastic relaxation. In contrast, the elongation of conservative repulsive force near the solid surface showed steeper temperature dependence than the bulk, which suggests that it was rate-limited by the attraction between the solid surface and the closest liquid molecules.

1. Introduction

Polymer melts have many unique characteristics, such as viscoelasticity and entanglement, which are not observed in low-molecular-weight compounds. The properties of polymer melts vary greatly depending on the degree of polymerization in addition to their chemical species (polyethylene, polyacetylene, polysiloxane, etc.). Large-molecular-weight polymer melts generally show high viscosity and take a long time to relax their molecules' conformation and mechanical response. In particular, those above around the critical molecular weight (M_c) exhibit significant non-Newtonian properties owing to the molecular entanglement.[1–3] Polymer melts are not only used as materials on their own but are often used in combination with other solid materials, such as for lubrication or fabrication of composite materials. In these applications, the interfaces between polymer melts and solids play crucial roles. Thus, molecular-scale analysis of both the structure and the mechanical properties of the interfaces with highly viscous polymer melts, especially above M_c, would be crucial.

Polymer melt/solid interfaces have been previously investigated by surface force apparatus (SFA)[4,5], X-ray reflectivity (XRR)[6–8], and static-mode atomic force microscopy (AFM)[9–11]. They have revealed that the layered density distribution exists temporarily at the interface and disappears with relaxation over time. However, SFA and XRR lack in-plane resolution and only provide the structural information averaged in a plane parallel to the solid surfaces. Since polymers have long molecular chains (10-100 nm) and each molecule has a structural degree of freedom, the averaged one-dimensional information is insufficient to analyze these interfaces' spatial structures. Also, XRR detects only periodic density distribution on the interface and does not provide information on mechanical properties. SFA and AFM are effective for mechanical property analysis because of their principle of detecting forces. However, static-mode AFM cannot individually detect the

conservative and dissipative components of the mechanical response, which corresponds to elasticity and viscosity. Since polymer melts have viscoelasticity, unlike low molecular weight liquids, it is essential to detect their viscosity and elasticity separately. Also, while static-mode AFM has a nanometer-scale in-plane spatial resolution, the previous studies are mostly limited to one-dimensional force-distance curve measurements just across under the tip, which cannot visualize the in-plane distribution of the mechanical properties based on liquid molecules. Therefore, a method capable of mapping interfacial structure and mechanical properties with high spatial resolution is needed.

Dynamic mode AFM, especially frequency modulation (FM-) AFM[12], would be a more powerful technique to detect conservative and dissipative interactions separately because it detects the interaction force as a change of resonance properties of the force sensor. FM-AFM has widely been applied for high-resolution structural analysis on solid/liquid interfaces.[13–16] In general, FM-AFM analysis in highly viscous liquids is difficult because the viscosity of the liquid depresses the resonant quality factor of sensors and the force sensitivity,[13] and most FM-AFM studies are limited to low-molecular-weight liquids[17–20]. To overcome this issue, we have developed FM-AFM utilizing a quartz tuning fork sensor (qPlus sensor[21,22]), which shows a higher quality factor than the conventional cantilevers even in a viscous liquid,[23] and have achieved FM-AFM analysis of the interface between silicone oil (poly(dimethylsiloxane); PDMS) with a viscosity of 970 mPa·s (number-average molecular weight M_n ~ 26000 from calculation[24]) and mica. We successfully imaged the atomic-scale topography of the solid surface and the layered density distribution on the interface, representing the molecules-layering structures in which the PDMS molecular chains are oriented parallel to the mica surface.[25]

With these backgrounds, the nanoscopic structures and mechanical properties of polymer melt/solid interface were analyzed by FM-AFM with high spatial resolution using the qPlus sensor in this study. PDMS with a 9750 mPa·s viscosity was employed as the model polymer, whose molecular weight (M_n ~ 59000) is far above M_c. Furthermore, we studied the time-temperature dependence of these relaxation processes. In general, the temperature dependence of relaxation processes is determined by the activation energy[26–28], which depends on its relaxation mechanism. The time-temperature dependence of bulk relaxation, such as macroscopic viscous flow[29] and local segmental motion[30], is well-studied for a wide range of polymers. However, it is not clear whether the relaxation process of the nanoscopic structures and mechanical properties on the interfaces also exhibit the time-temperature dependence similar to the bulk relaxation. Therefore, analyzing and determining the temperature dependence of molecular-scale relaxation phenomena on the interface are essential for revealing the mechanisms of relaxation processes both on the interface and in bulk. In addition, to the author's knowledge, FM-AFM analysis in such a highly viscous liquid has yet to be reported. Therefore, this study is also crucial in terms of the progress of the AFM techniques in highly viscous liquids, as well as insights into the interfacial physical chemistry of polymer melts and solids.

Methods

Poly(dimethylsiloxane) (PDMS) was employed as a model polymer melt. Figure 1 shows the molecular structure of PDMS. It is a silicone oil with a straight-chain structure and exhibits a wide range of viscosities depending on molecular weight and chain length. We used a PDMS oil (KF-96-10000cs, Shin-Etsu Chemical Co., Ltd.) as received. The viscosity was η=9750 mPa·s at 25 ℃ (room temperature) and 3790 mPa·s at 80 ℃, which was measured by a viscometer (Kyoto Electronics Manufacturing Co., Ltd., EMS-1000). The molecular weight and chain length were calculated[24] as M_n = 59000 and l =250 nm, respectively.

Cleaved muscovite mica [$KAl_2(Si_3Al)O_{10}(OH)_2$] substrates were used as substrates, which have been used for high-resolution FM-AFM imaging in various liquids, and the atomically flat surface can easily be obtained by cleavage.

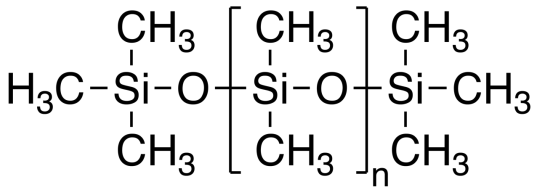

Figure 1. The structural formula of poly(dimethylsiloxane) (PDMS). $n \sim 800$ was used for the experiment.

The experiment was performed by a system based on a commercial AFM (JEOL Ltd., JSPM-5200) with a homebuilt AFM head for qPlus sensors. The qPlus sensor was built using a quartz tuning fork (QTF; purchased from SII Crystal Technology Inc.) with resonant frequency f_0 = 32.768 kHz and spring constant k = 1890 N m^{-1} (calculated from its shape). One prong of QTF

was fixed on the mount, and a tungsten tip was mounted on the end of the free prong of QTF by epoxy resin (EPO-TEK H70E; Epoxy Technology Inc). The probe was fabricated from tungsten wire (Nilaco Co., diameter = 0.10 mm) by electrochemical etching in 1.0 mol L^{-1} potassium hydroxide solution. The radius of the tip was approximately less than 100 nm, as measured by FE-SEM inspection.

The AFM was used with frequency modulation (FM) mode[12]. The sensor was mechanically vibrated at its resonance frequency by a lead zirconate titanate (PZT) piezoelectric plate attached to the sensor clamp, and the deflection of the sensor was detected as a signal from the QTF amplified by a low noise differential amplifier invented by Giessibl et al.[31]. The sensor was self-excited at its resonant frequency by a PLL-excitation loop using a digital lock-in amplifier (MFLI, Zurich Instruments), which is also used for the detection of the resonance frequency shift (Δf) and the vibrating amplitude ($A_{\text{p-p}}$). The vibrating amplitude of the sensor $A_{\text{p-p}}$ was kept constant during the AFM experiments by automatic gain control using a PID controller in the lock-in amplifier. The energy dissipation E_{d} and the increase of the viscous damping factor of tip vibration $\Delta\gamma$ were calculated from the excitation voltage applied for the constant amplitude of sensor deflection[32].

Δf-z (frequency shift versus distance) curves were obtained by scanning the probe along a path perpendicular to the solid surface in approaching and retracting direction, and the corresponding $\Delta\gamma$-z (damping factor versus distance) curves were obtained simultaneously by tracing $\Delta\gamma$ during the Δf-z curves measurement. Also, the cross-sectional two-dimensional (2D) Δf maps in the vertical plane to the substrate were obtained by doing these measurements sequentially on each horizontal point across the lateral path.

Approximately 0.5 μL of PDMS was dropped onto 1 × 1 cm^2 mica substrates in a dry chamber (dew point < -50 ℃) and then spin-coated in an ambient condition to spread over the surface of

the substrates, which is to reduce the probe's immersion length in the liquid since the resonant quality factor of sensors decreased by increasing the immersion length[25]. The speed and duration for spin-coating were 2000 r min^{-1} and 90 min, as determined for the minimum duration required to spread PDMS over the entire substrate. The thickness of the liquid film measured by AFM was about 5 μm, which agreed well with the theoretically calculated value[33]. The spin-coated substrates were settled at room temperature or annealed at 80 ℃ (heated by a hot plate) for a specific time in a dry chamber, then investigated by qPlus AFM in an ambient condition at room temperature.

Results and Discussion

Figure 2(a) shows a cross-sectional 2D Δf map obtained at the interface after spin-coating and settling for 29 h at room temperature. Δf-z curves obtained along line AB in (a) were shown in Figure 2(b). The curves acquired during the tip approach and retraction are shown in red and blue, respectively. Note that all the Δf-z curves in this paper were averaged over 25 adjacent curves to improve the signal-to-noise ratio and further smoothed with a moving average filter. In addition, the amplitude error of the sensor deflection was successfully kept to less than ±10 %, and no oscillatory error was observed in amplitude-z curves for all experiments.

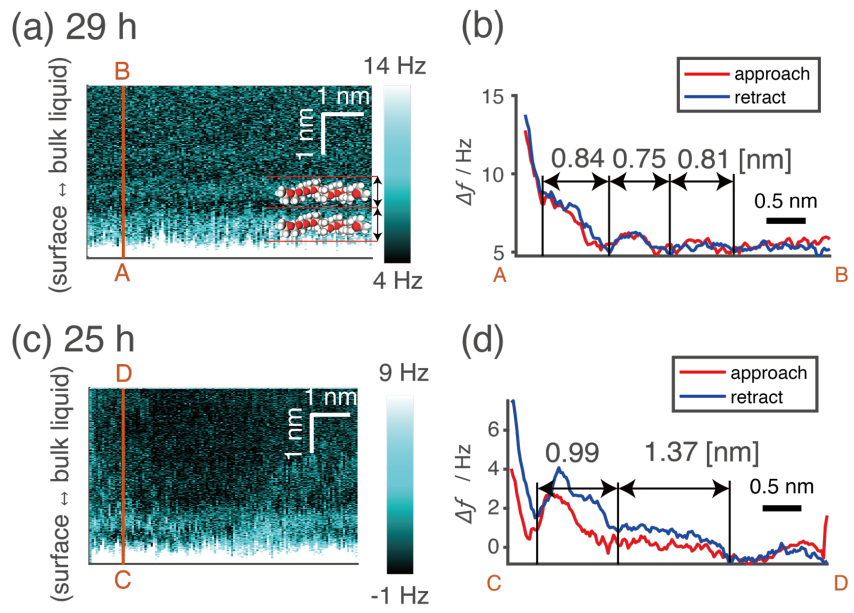

Figure 2. (a, c) 2D Δf map (approach) and (b,d) Δf-z curves obtained after settling for (a, b) 29 h and (c,d) 25 h at room temperature, respectively. The measurement parameters: (a, b) f_0 = 17732 Hz, Q=612, $A_{p\text{-}p}$ = 274 pm. (c, d) f_0 = 17053 Hz, Q = 651, $A_{p\text{-}p}$ = 269 pm.

After 29 h of settling, the layered Δf contrast parallel to the mica substrates was visualized on the 2D Δf map (Figure 2(a)). This layered contrast corresponds to the periodic oscillation of the Δf-z curves (Figure 2(b)), and their period was about 0.7-0.9 nm. This period is roughly equal to the diameter of PDMS molecular chains and matches the distance between the molecular chains of 3170 mPa·s PDMS obtained from the theoretical calculation (PRISM; polymer reference interaction site model), molecular dynamics simulation, and X-ray diffraction[34]. It also corresponds to the interplanar spacing of cold-crystallized PDMS with a viscosity (25 °C) of 3060, 13700 mPa·s[35].

Since Δf is the convolution of the gradient of the conservative force F_{cons} with weighting by displacement over a vibration cycle and the F_{cons} is the gradient of its potential, the oscillation of

Δf indicates a similar oscillation of F_{cons} and the corresponding potential. To convert the F_{cons} distribution to the density distribution of low-molecular-weight compounds such as water, the solvent tip approximation (STA)[36,37] has been used. Although it cannot be directly applied to polymer melts because of the molecular size of the polymer (length > 100 nm), the periodic distribution in the tip potential qualitatively indicates the existence of corresponding periodic density distribution with approximately the same period. Therefore, it can be concluded that PDMS molecules formed a layered density distribution with a period of 0.7-0.9 nm near the mica surface, which suggests that the main chains of PDMS molecules near the mica surface were oriented parallel to the solid surface. This result is well consistent with a previous static-mode AFM study performed on a 480 mPa·s PDMS/SiO_2 interface[9] and our previous qPlus FM-AFM study performed on a 970 mPa·s PDMS/mica interface.[25] Furthermore, the curves acquired during the tip approach (red) and retraction (blue) were well consistent. Generally, in Δf-z curve measurements and 2D Δf mapping at solid-liquid interfaces, the tip perturbs the liquid distribution when approaching the tip. Therefore, the result that the curves coincided during the approach and retraction suggests that the layered structure on the interface was stable or metastable.

Figure 2(c) shows a cross-sectional 2D Δf map obtained at the interface after spin-coating and settling for 25 h at room temperature. Although the layered Δf distribution was imaged for the 29 h-settling sample (Figure 2(a)), a disordered Δf distribution was imaged for the 25 h-settling sample. A Δf-z curve obtained along line CD in (c) was shown in Figure 2(d). Both approaching and retracting curve fluctuated with a period of 0.9 to 1.4 nm, and these curves were not consistent. This period was larger than that obtained on the 29 h-settling sample. The disordered structure and the inconsistency between the two curves can be regarded as an incomplete state before reaching the layered structure observed on the 29 h-settling sample. This result suggests the following two

possibilities. The first one is that the formation of the layered distribution takes more than 25 h. As shown in Figure 2(a), a layered distribution was observed in 29 h, and the difference in time was not significant. Another possibility is that the in-plane distribution was not uniform. That is, at 25-29 h after spin coating, both regions with the layered distribution and the disordered regions exist. However, as shown in Figures 2(b) and 2(d), the Δf-z curves obtained on the layered structure during the approach and the retraction were well consistent, whereas the curves obtained on the disordered region were not. This suggests that the layered structure is metastable or stable. Also, the fact that the layered structure observed after a longer settling time (Figure 2(a)) is reasonable from the viewpoint that a more stable structure would be formed by increasing the settling time.

In contrast, the previous static-mode AFM study performed on 480 mPa·s PDMS/Si interface showed that the oscillatory force profile was observed soon after the deposition of the PDMS ($\leq$ 30 min).[9] This difference can be explained by the entanglement of the PDMS molecules. In general, the effects of entanglement on the bulk physical properties become significant for the polymers with the critical entanglement molecular weight M_c. The viscosity of the bulk liquid increases drastically above M_c.[38] The M_c of PDMS is approximately 21,000-33,000,[39] which corresponds to the viscosities of about 590-1200 mPa·s.[24] Therefore, the PDMS used in this experiment has a much higher molecular weight than M_c, whereas that used in the previous report with static-mode AFM[9] has a lower molecular weight than M_c.

Supposing the critical entanglement molecular weight can be applied to the molecules forming these layering structures, the difference in their formation time above and below M_c can be explained by the difference in the limitation of molecular motion. The entanglement of polymers with molecular weights below M_c can be almost ignored, and the molecular motion is explained

by the Rouse model[40] (bead-and-spring model) without entanglement. In this situation, the motion of the polymer molecules at the solid-liquid interface is not limited by anything other than the conformation of the molecule, and the molecular segments on the interface can freely move and exchange their position with other segments. In contrast, the molecules with a molecular weight above M_c cannot move freely in the entangled molecular chain networks, and their motion is mainly limited to reptation[41], in which the molecules move in the longitudinal direction through tunnels in the network. This limitation retards the movement and rearrangement of the molecules, which can delay the formation of the layered density distribution on the interface. This can explain the slow formation of the layered distribution of the molecules, which is not similar to the PDMS with a lower molecular weight than M_c.

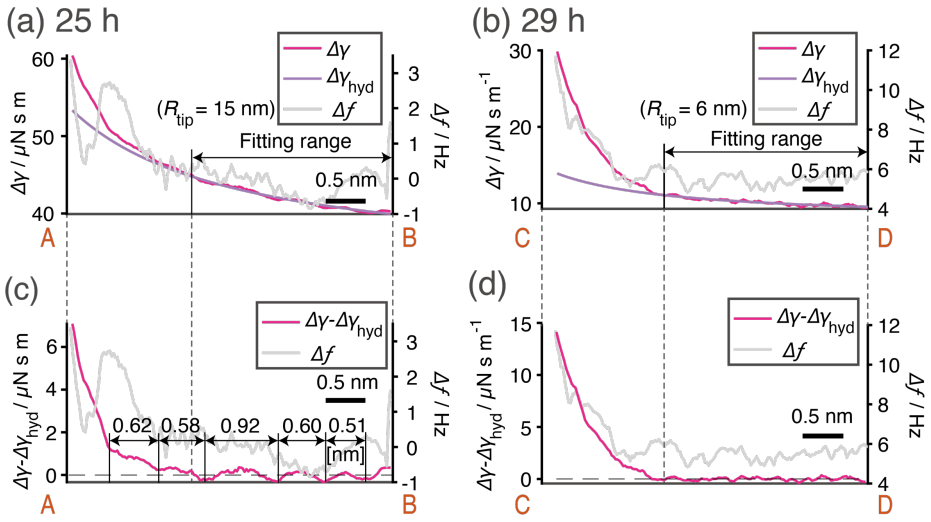

Figure 3. (a, b) $\Delta\gamma$-z curves and the fitted $\Delta\gamma_{hyd}$-z curves obtained after (a) 25 h, (b) 29 h of settling at room temperature. The fitting range and the fitted R_{tip} values are also shown. (c, d) The residual $\Delta\gamma$-$\Delta\gamma_{hyd}$ versus z curves corresponding to (a, b), respectively.

(a, c) f_0 = 17732 Hz, Q=612, $A_{p\text{-}p}$ = 274 pm. (b, d) f_0 = 17053 Hz, Q = 651, $A_{p\text{-}p}$ = 269 pm.

To discuss the mobility of the liquid molecules in more detail, we obtained $\Delta\gamma$-z curves simultaneously with the Δf-z curves. Figures 3(a) and (b) show $\Delta\gamma$-z curves obtained on the 25 h-settling and 29 h-settling samples, respectively. $\Delta\gamma$ increased as the tip approached the solid surfaces for both samples. $\Delta\gamma$ is the superposition of the dissipative interaction between the tip and the interfacial structure and the background hydrodynamic interactions originating from the squeeze-out of the bulk liquid induced by tip movement. If the liquid on the interface can be regarded as a homogeneous isotropic fluid, $\Delta\gamma$ can be expressed by the hydrodynamic component $\Delta\gamma_{hyd}$. Under the assumption that the $\frac{z}{R_{tip}}$ and the Reynolds number Re are sufficiently small, $\Delta\gamma_{hyd}$

is described with the viscosity η, the tip radius R_{tip}, and the distance to the solid surface z as follows:[42]

$$\Delta\gamma_{\mathrm{hyd}} = 6\pi\eta\frac{{R_{\mathrm{tip}}}^2}{z} \quad (1)$$

Note that, $Re \sim \frac{\rho z}{\eta} A\omega \leq 2 \times 10^{-12} \ll 1$ and $\frac{z}{R_{\mathrm{tip}}} \leq 10^{-1} \ll 1$ for z = 1 nm in this experiment, this assumption is reasonable.

Because $\Delta\gamma_{\mathrm{hyd}}$ is based on the viscosity of the bulk liquid, we carried out the fitting for the z range relatively away from the solid surface. The fitted $\Delta\gamma_{\mathrm{hyd}}$ are also shown in Figures 3 (a) and 3 (b). The residual $\Delta\gamma$ - $\Delta\gamma_{\mathrm{hyd}}$ can be regarded as originating from the dissipative interaction between the tip and the interfacial structure. Figure 3(c) and (d) are the residual $\Delta\gamma$-$\Delta\gamma_{\mathrm{hyd}}$ versus z plots corresponding to Figure 3(a) and (b). $\Delta\gamma$-$\Delta\gamma_{\mathrm{hyd}}$ increased as the tip approached the sample surface for both samples. The region where $\Delta\gamma$-$\Delta\gamma_{\mathrm{hyd}}$ increased was 1-2 nm from the nearest point to the solid surface, which corresponds to the first to the second layer of the solvation layers observed in the Δf-z curve. Since $\Delta\gamma$ in FM-AFM generally indicates the friction coefficient, the increase in $\Delta\gamma$ near the surface corresponds to an increase in the local viscosity of the liquid. Since the viscosity of liquid reflects the mobility of molecules,[43] the increase in the local viscosity along the solid surface indicates that the molecular mobility nearest to the solid surface is limited, which implies the intense attraction between the solid surface and the closest liquid molecules.

In addition, $\Delta\gamma$-$\Delta\gamma_{\mathrm{hyd}}$ obtained on the 25 h-settling sample (Figure 3(c)) showed the oscillation of $\Delta\gamma$ with a period of 0.5-1.0 nm, which is roughly equal to the diameter of PDMS molecules. Hofbauer *et al.* reported an FM-AFM study on an alcohol/graphite interface and showed that both Δf and $\Delta\gamma$ oscillated at the interface. The $\Delta\gamma$ oscillation was explained by the presence of the "solid-like" (crystallized) solvation layers and the squeezing-out of the liquid molecules with low mobility.[20] Therefore, the $\Delta\gamma$ oscillation observed in Figure 3(c) may reflect the low mobility of

the molecules on the interface. However, the oscillation period of $\Delta\gamma$ was inconsistent with that of Δf, reflecting the density distribution, and this oscillation was not observed in the layered distribution region on the 29 h-settling sample (Figure 3(d)). To clarify the origin of the oscillation, further AFM study on polymer melt/solid interfaces would be required.

The results described above indicate that the layered distribution is either a stable or metastable structure. To confirm either of these, samples that had settled for a more extended period of time were analyzed. Figure 4(a) and (b) are the obtained 2D Δf maps after 74 and 142 h of settling at room temperature, respectively. A Δf-z curve obtained along line EF in Figure 4(a) and that obtained along line GH in Figure 4(b) are shown in Figure 4(c) and (d), respectively. Figure 4(e) and (f) are the $\Delta\gamma$-$\Delta\gamma_{hyd}$ versus z curves corresponding to each Δf-z curve of Figure 4(c) and (d), respectively.

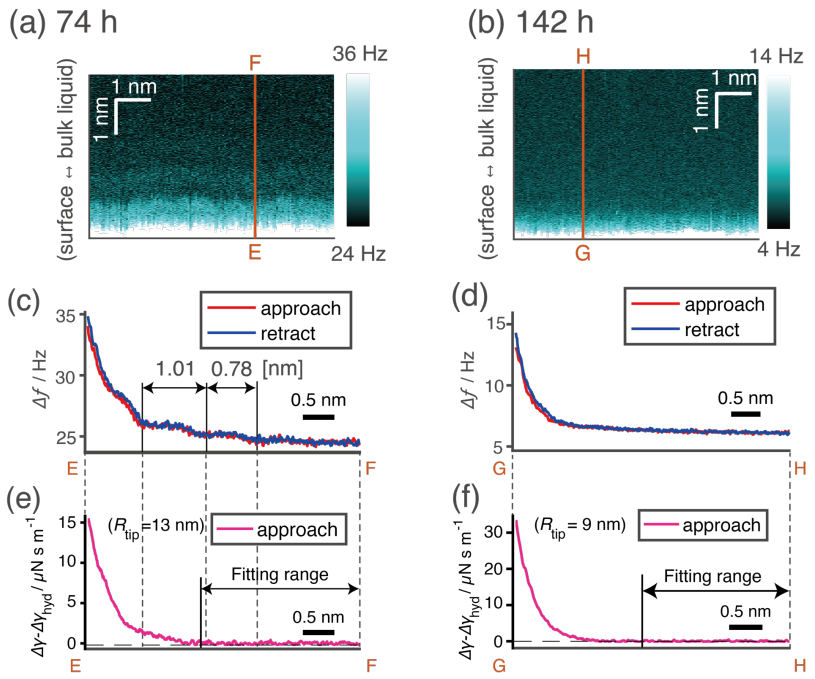

Figure 4. (a, b) 2D Δf map (approach), (c, d) Δf-z curves, (e, f) $\Delta\gamma$-$\Delta\gamma_{hyd}$ versus z curves obtained after (a, c, e) 74 h, (b, d, f) 142 h of settling at room temperature after spin-coating. (a, c, e) f_0 = 16439 Hz, Q = 480, $A_{p\text{-}p}$ = 307 pm. (b, d, f) f_0 = 15262 Hz, Q = 579, $A_{p\text{-}p}$ = 313 pm.

The layered contrast in the 2D Δf maps (Figure 4(a) and (b)) became less visible with increasing settling time. Correspondingly, the Δf-z curves (Figure 4(c) and (d)) changed into almost monotonic curves, with only weak oscillation at 74 h and no oscillation at 142 h of settling. The $\Delta\gamma$-$\Delta\gamma_{hyd}$ versus z curves (Figure 4(e) and (f)) were monotonic in both settling times and showed no oscillation, similar to 29 h of settling. Also, $\Delta\gamma$-$\Delta\gamma_{hyd}$ increased in the region of 1-2 nm from the nearest point to the solid surface, as in the case of 29 h of settling.

Sun *et al.* reported a static-mode AFM study on 480 mPa·s PDMS/silicon oxide interface, showing that the layered interfacial structure disappeared in ~20 h.[9] This disappearance was explained as a structural relaxation from a layered distribution to a random-coiled configuration

of the PDMS.[9] The disappearance of the layered Δf distribution in our study can be explained in the same way. The relaxation time of 9750 mPa·s PDMS on mica was 74-142 h in our study, while those of 97 mPa·s PDMS on Si[7] and 480 mPa·s PDMS on silicon oxide[9] was ~4 h and ~20 h, respectively. That is, these results indicate that the relaxation time required for disappearing the layered distribution increases with the viscosity. Note that, in this experiment, the shear caused by the spin coating might be an additional cause of the persistence of this structure for a long time, but this is unlikely because no significant difference in the Δf and $\Delta\gamma$ distribution was observed with or without spin coating in the experiment using PDMS with a viscosity of 970 mPa·s (Supporting Information: Figure S1).

To obtain further insight into the relaxation process on the interface, we investigated interfacial structure after heating the sample. We prepared two PDMS/mica samples for heating; one was heated for 5.7 h at 80 °C and the other for 16 h at 80 °C. After the heating, both samples were settled for 24 h at room temperature, and the interface was investigated by the AFM. Figure 5(a) and (b) are the obtained 2D Δf maps of the 5.7 h-heated sample and 16 h-heated sample, respectively. A Δf-z curve obtained along line IJ in Figure 5(a) and that obtained along line KL in Figure 5(b) are shown in Figure 5(c) and (d), respectively. Figure 5(e) and (f) are the $\Delta\gamma$-$\Delta\gamma_{hyd}$ versus z curves corresponding to Δf-z curves of Figure 5(c) and (d), respectively.

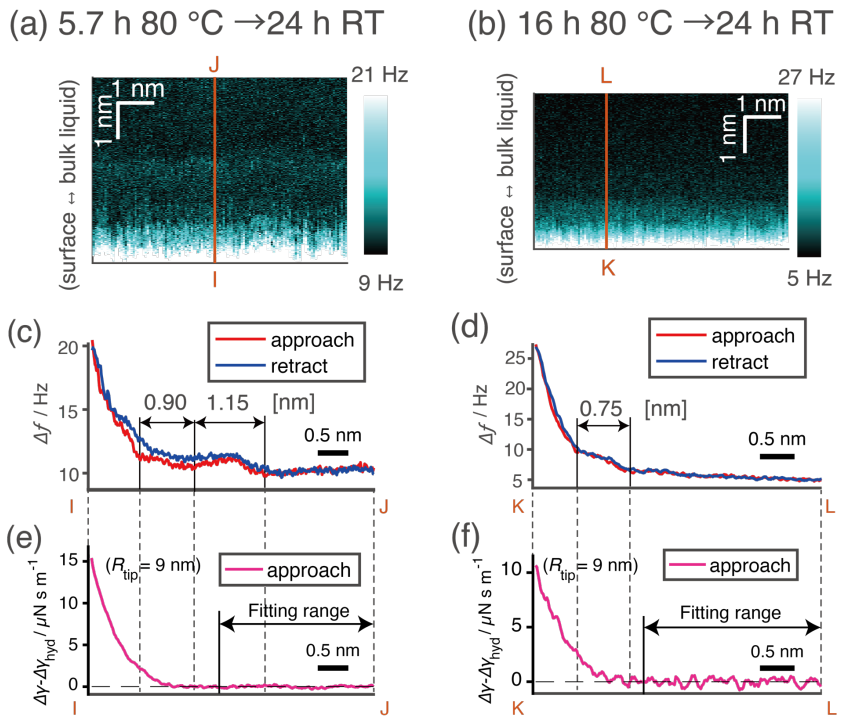

Figure 5. (a, b) 2D Δf map (approach), (c, d) Δf-z curves, (e, f) $\Delta\gamma$-$\Delta\gamma_{hyd}$ versus z curves obtained after heating for (a, c, e) 5.7 h and (b, d, f) 16 h at 80 ℃ and then settled at room temperature for 24 h after spin-coating.

(a, c, e) f_0 = 16687 Hz, Q = 694, $A_{p\text{-}p}$ = 266 pm. (b, d, f) f_0 = 17119 Hz, Q = 769, $A_{p\text{-}p}$ = 304 pm.

Both the 5.7 h-heated sample and the 16 h-heated sample showed weaker oscillation of Δf than the 29 h-settled sample shown in Figure 2(b), and the Δf-z curve of the 16 h-heated sample showed a slight oscillation of only one time. However, the weak oscillation of Δf was still visible after 16 h of heating, in contrast to that for 142 h of settling at room temperature. The $\Delta\gamma$-$\Delta\gamma_{hyd}$ versus z curves were monotonic without oscillations for both heating time and showed an increase in the region of 1-2 nm from the nearest point to the solid surface, as in the cases of settling at room temperature.

To independently discuss the oscillatory and monotonically increasing components in the Δf-z curves, we separate Δf-z curves into the short-range and long-range components by curve fitting. The long-range component Δf_{long} is the one that monotonically increases with approaching the solid surface, which was assumed to be described by a double-exponential function $ae^{-bz} + ce^{-dz} + h$ (a, b, c, d, h: arbitrary constants, z: relative distance from the solid surface). By fitting the Δf-z curve with this function form, the Δf_{long}-z curve was obtained as the double-exponential curve with the fitted coefficients a, b, c, d, and h. The double-exponential functional format was used because it approximated the Δf-z curve well and provided only negligible residuals other than the periodic Δf oscillations. This function has also been empirically used for approximating the force-distance curve obtained by static-mode AFM[44]. Therefore, the residual Δf-Δf_{long} practically contains only the oscillation derived by the layering interfacial structures, which was taken as a short-range oscillatory component $\Delta f_{\mathrm{short}}$.

Figure 6 shows ~~is~~ the (a, b) $\Delta f_{\mathrm{short}}$-$z$ and the (e, f) Δf_{long}-z curves for the samples with or without heating, respectively. (Figures 6(b) and (f) also contain the curve for 29 h of settling without heating for comparison.) Each $\Delta f_{\mathrm{short}}$-$z$ and Δf_{long}-z curves were transformed into the corresponding conservative force, $F_{\mathrm{cons,\ short}}$-$z$, $F_{\mathrm{cons,\ long}}$-z by Sader's transformation.[45] It is known that Δf depends on the vibrating amplitude, and the relationship between density distribution and force has been well studied, though limited to small molecule liquids[36,37,46]. $F_{\mathrm{cons,\ short}}$-$z$ and $F_{\mathrm{cons,\ long}}$-z curves are shown in Figures 6(c, d) and 6(g, h), respectively.

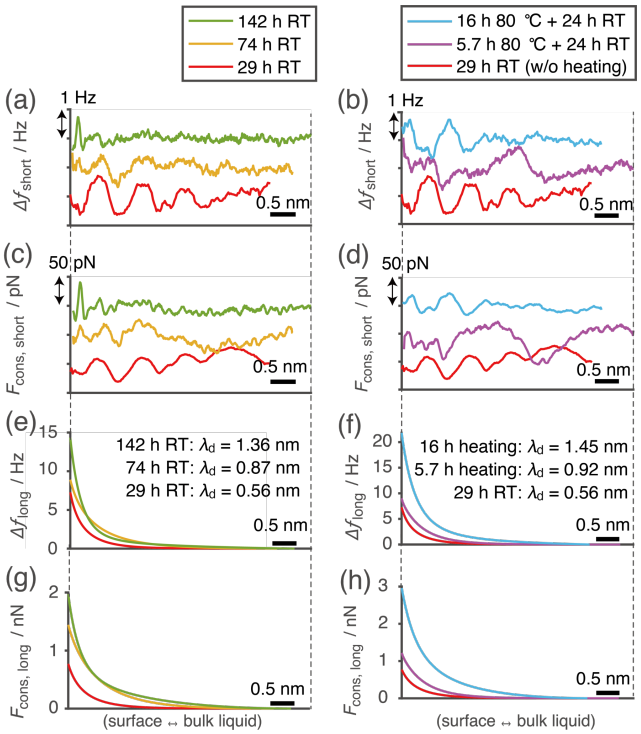

Figure 6. (a, b) Δf_{short}-z, (c, d) $F_{\text{cons, short}}$-z, (e, f) Δf_{long}-z, (g, h) $F_{\text{cons, long}}$-z curves transformed from each curve in Figures 2, 4, and 5. (a, c, e, g) settled for 29, 74, 142 h at room temperature, (b, d, f, h) heated for 5.7 h, 16 h at 80 ℃, then settled for 24 h at room temperature (with the data for 29 h settling at RT for comparison). The definition of the decay length λ_d is in the text.

After 29 h of settling at room temperature, Δf_{short}-z (Figure 6(a)) and $F_{\text{cons, short}}$-z (Figure 6(c)) curves showed the clear three oscillatory peaks, which corresponds to the presence of layered distribution on the interface. The amplitude of the oscillation was suppressed after 74 h of settling at room temperature, and almost no oscillation was observed after 142 h of settling (Figures 6(a) and (c)). This indicates the layered density distribution of the liquid molecules on the interface disappeared after settling at room temperature for 142 h. In contrast, after heating for 5.7 and 16 h at 80 ℃, both Δf_{short}-z (Figure 6(b)) and $F_{\text{cons, short}}$-z (Figure 6(d)) curves still showed the fluctuation,

indicating that the weakened layered density distribution remained even after 16 h of heating at 80 °C.

In the fitting function of the double-exponential form $\Delta f_{\mathrm{long}} = ae^{-bz} + ce^{-dz} + h$ $(b > d)$, the values of a, c, and h depend on the offsets on the Δf and z. Especially since the offset of z cannot be determined explicitly in the FM-AFM in principle, it is difficult to compare and discuss the coefficients of a, c, or $F_{\mathrm{cons,\ long}}$, Δf_{long}-z curves themselves. However, the values of b and d do not depend on the offset of z and provide the decay length of the interaction force. As the Supporting Information: Figure S2 shows, the Δf_{long} was mainly represented by the term with longer decay length with the offset ($ce^{-dz}+h$), and the inverse of d ($\lambda_d=1/d$) can be regarded as the decay length of the long-range interaction on Δf_{long}. Note that, since Δf for $F_{\mathrm{cons}} = F_{\mathrm{cons}}^{z=0} e^{-z/\lambda}$ is calculated to be $\Delta f = ce^{-z/\lambda}$ ($c = \frac{f_0}{\pi k A} e^{-A/\lambda} I_1\left(\frac{A}{\lambda}\right) =$ const., $I_1(x) = \frac{1}{\pi}\int_0^{\pi} e^{x\cos\theta}\cos\theta \ d\theta$), the exponentially decaying Δf_{long} corresponds to a long-range repulsive conservative force $F_{\mathrm{cons,\ long}}$ following an equal decay length λ_d. The calculated λ_d is shown in Figure 6(e, f) for each Δf_{long}-z curve. The value of λ_d was provided as the average of the approaching and retracting scan. The λ_d increased after the duration of settling at room temperature (Figure 6(e)) or heating at 80 °C (Figure 6 (f)). This result indicates that the long-range component of the F_{cons} ($F_{\mathrm{cons,\ long}}$) has changed to act over a longer distance. Moreover, 5.7 and 16 h-heated samples showed larger λ_d than 74 and 142 h-settling samples, respectively. This means that the disappearance of periodic density distribution reflected in $\Delta f_{\mathrm{short}}$ and the increase of the decay length λ_d for the long-range repulsive conservative force $F_{\mathrm{cons,\ long}}$ showed different time-temperature dependence in terms of relaxation time.

Note that, since the polymer melt also shows significant elasticity with high viscosity, the elasticity of the liquid can also cause a long-range increase in Δf and F_{cons}, not only the density

distribution. In fact, the previous quasi-elastic neutron scattering (QENS) on silica-particle-filled PDMS has suggested that a ~5 nm thick layer of liquid molecules is formed on the silica surface, which forms a strong interaction with the surface and brings the extra elasticity of the interface.[47] On the other hand, from the standpoint of solvent tip approximation (STA), the relationship between the conservative forces and the density distribution can be formulated as follows:[36,37]

$$F_{\mathrm{cons}}(z) = \frac{k_{\mathrm{B}}T}{\rho(z)}\frac{d\rho(z)}{dz} \tag{2}$$

For $F_{\mathrm{cons,\ long}}(z) = Ce^{-z/\lambda_d}$, the corresponding density distribution is calculated as $\rho(z) = \rho_0 e^{-\lambda_d C \exp[-z/\lambda_d]/(k_{\mathrm{B}}T)}$. That is, the apparent density decreases near the solid surface. The XRR analysis also proved that the liquid molecules show a lower density near the solid surface in 1-3 nm on PDMS/Si interface.[6] They considered the low-density layer detected by XRR and the highly elastic layer observed by QENS to be identical, which is widely known as the "immobilized layer"[48]. Therefore, the increase in $F_{\mathrm{cons,long}}$ near the solid surface would reflect either a lower density or the increased elasticity near the solid surface, or both, which are strongly related to each other.

The temperature dependencies of bulk viscoelastic relaxation time $\tau(T)$ are described by the time-scale shift factor $a_{T,\eta}$, which can be calculated from the viscosity $\eta(T)$ for the different absolute temperature T and T_0 ($T < T_0$) with the density $\rho(T)$:[27,49]

$$a_{T,\eta} = \frac{\tau(T)}{\tau(T_0)} = \frac{\eta(T)}{\eta(T_0)}\frac{T_0\rho(T_0)}{T\rho(T)} \tag{2}$$

The shift factor of relaxation processes reflects the activation energy derived from the main rate-limiting mechanisms. The apparent activation energy ΔE of the relaxation process can be calculated as follows (R: gas constant):[43]

$$a_T = \exp\left[\frac{\Delta E}{R}\left(\frac{1}{T} - \frac{1}{T_0}\right)\right] \quad (3)$$

As mentioned in the experiment section, the obtained bulk viscosity was 3790 mPa·s at 80 ℃ and 9750 mPa·s at 25 ℃. The density of PDMS is reported to be 0.922 g cm^{-3} at 80 ℃ and 0.969 g cm^{-3} at 25 ℃[50]. From these values, the shift factor $a_{T,\eta}$ and the activation energy E_η of viscous flow at $T_0 = 80 + 273$ [K] and $T = 25 + 273$ [K] was calculated to be $a_{T,\eta} = 2.9$ and $E_\eta = 17$ kJ mol^{-1}. That is, taking the time-temperature superposition principle[27,51,52], heating at 80 ℃ for 1 hour is equivalent to settling at room temperature (25 ℃) for 2.9 h in terms of bulk viscoelastic relaxation. Therefore, the 5.7 h and 16 h of heating with the subsequent 24 h settling are calculated to be equivalent to settling for 40 h and 70 h at room temperature in the bulk viscoelastic relaxation, respectively.

Note that, the apparent activation energy ΔE is not always constant nor independent of the temperature. For bulk viscoelasticity, the activation energy of viscous flow ΔE_η is calculated as the function of temperature with Williams-Landel-Ferry (WLF) parameters.[27] However, ΔE_η converges to a constant value at higher temperatures than the glass transition temperature T_g,[27,49] and the temperature dependence of ΔE_η can be practically ignored for small temperature differences at $T > T_g + 100$ K.[49] Since T_g of PDMS is -123.3 ℃[53,54], ΔE_η can be regarded to be constant.

Regarding the oscillation in the Δf_{short}-z and $F_{cons,\,short}$-z curves, no obvious difference was found in amplitude between the sample heated for 16 h and the sample left at room temperature for 74 h, though the Δf_{short} oscillation of the 142 h-settling sample almost disappeared. Taking the interpretation that 74 h of settling at room temperature is equivalent to 16 h of heating with subsequent 24 h of settling, the shift factor $a_{T,\,short}$ and the activation energy ΔE_{short} are calculated

to be $a_{T,\,\mathrm{short}}$ = (74-24)/16 = 3.1 and E_{short} = 18 kJ mol^{-1}. These values are almost similar to those of the bulk viscoelastic relaxation ($a_{T,\,\eta}$=2.9 and E_{η} =17 kJ mol^{-1}).

On the other hand, the increase of λ_{d} in the Δf_{long}-z and $F_{\mathrm{cons,\,long}}$-z curves showed more steeper time-temperature dependence. Since the 16 h-heated sample showed a similar λ_{d} value to the 142 h-settling sample, the shift factor $a_{T,\mathrm{long}}$ and the activation energy ΔE_{long} of λ_{d} elongation are calculated to be $a_{T,\,\mathrm{long}}$ =(142-24)/16 = 7.4 and E_{long} = 32 kJ mol^{-1}, which are obviously larger than $\Delta E_{\mathrm{short}}$, $a_{T,\,\mathrm{short}}$ and ΔE_{η}, $a_{T,\,\eta}$. This suggests that the elongation rate of λ_{d} is determined by a different mechanism from the suppression of the short-range oscillatory component or the bulk viscous relaxation.

The attraction between the charge sites on the solid surface and the dipole of the PDMS molecules is one of the possible mechanisms that can delay the interfacial relaxation. Although PDMS is a nonpolar molecule, a dipole is induced when it contacts with a charged mica surface. The relaxation model based on the charge sites/molecular segments attraction has already been predicted[6,9] to explain the long-range increase in the repulsive force in AFM force-distance curve[9] and the formation of "immobilized" layer of lower density[6] near the solid surface on the interface. As mentioned above, after 29 h of the contact at room temperature, the molecules near the solid surface were oriented parallel to the solid surface, forming a layered density distribution (Figure 2(b)). However, the charge-dipole interactions are broken at a particular rate by the thermal motion of the molecules, and the other molecules replace the molecular chain segments on the charge sites if the vacant sites make a new bond with the different molecular segments. This displacement proceeds irreversibly due to the conformational entropy gain because the released chain segments by the substitution can form a three-dimensional conformation. After this displacement progresses, the number of PDMS molecules directly attracting the solid surfaces is increased, and only partial

segments of the PDMS molecules interact with the charge sites. In this situation, the volume occupied by the PDMS molecules that directly attract the solid surfaces also increases. Note that, since the molecular chain length of PDMS used in this study is as long as 250 nm, the molecular motion of the segments not interacting with the solid surface is also limited when the other segments are making charge-dipole bonds. Thus, the increased volume occupied by these molecules suppresses molecular mobility over longer distances. Since the lower molecular mobility at the interface results in an excess of both viscosity and elasticity at the interface compared to the bulk, an increase in the number of molecules interacting with the solid surface increases the decay length λ_d of the long-range repulsive force $F_{cons,\,long}$. In addition, As mentioned above, the increase in $\Delta\gamma$-$\Delta\gamma_{hyd}$ near the solid surface (Figures 3(c, d), 4(e, f), 5(e, f)) demonstrated the low mobility of the molecules in the layers closest to the solid surface. This result also suggests that the charge-dipole interaction on the closest layer is strong and limits the mobility of the molecular segments directly interacting with solid surfaces. Therefore, the fact that the activation energy of the λ_d elongation ΔE_{long} was significantly larger than ΔE_η was most likely based on the substitution of charge-dipole bond.

Further, the previous studies have associated the growth in strength of long-range repulsive force with the disappearance of the periodic density distribution as follows: The periodic layered structures are initially formed due to the contact of the polymer melt/vacant solid surface or the shear flow during casting into the AFM cell, and disappear because they are the unstable structures. The interfaces then become occupied by randomly coiled segments, which include those that have detached from the solid surface.[9] Although this explanation does not assume a delayed formation of the layered structure above M_c or the fact that the layered structure is metastable, a similar interpretation consistent with our results is possible with some modifications based on the

segmental substitution on the solid surface. The layered structure is metastabilized by the solid surface / liquid molecule interaction on the closest layer and the intermolecular interactions between the layers. After the substitution process on the closest layer, the segments released from the solid surface make the loops and tails. Since these structures act as conformational obstacles for maintaining the layered density distribution, the substitution process on the closest layer destabilizes the layered structure. This causes the stability of the layered structure on the interface to decrease over time, resulting in random coiling on the interface.

Considering that these substitution and destabilization processes include the breaking process of charge-dipole bonds between the closest layer and the solid surface, the disappearance rate of the layered structure could also be dominated by the activation energy to break the charge-dipole bonds, which is larger than that for the bulk viscous flow. Nevertheless, as mentioned above, the activation energy of the disappearance of the layered structure was almost equal to the bulk viscous flow. This fact implies that the rate of disappearance of the layered structure was mainly dominated by the activation energy of bulk viscous flow rather than that of breaking the charge-dipole bond. It may be counterintuitive that a step of smaller activation energy would be the rate-limiting reaction. However, this result is not strange because the rate of the reaction depends not only on the activation energy but also on the frequency factor in the Arrhenius equation. The relationship between the shift factor and activation energy shown in eq. (3) is based on the Arrhenius equation,[43] which describes the reaction rate constant k with the frequency factor A and the activation energy ΔE as $k = A\exp\left(-\frac{\Delta E}{RT}\right)$. It is impossible to determine the frequency factor or rate constant in this experiment since the shift factor reflects only the activation energy. If the disappearance of the layered structure is regarded as a sequential reaction, the overall reaction rate k is determined by the elementary reaction with the smallest rate constant. That is, it is possible

for a process with low activation energy, i.e., bulk viscous flow, to be the rate-limiting process depending on the frequency factor. The disappearance of the layered structure is attributed to both the segmental substitution on the solid surface and the random coiling of the PDMS molecules. Because the molecular chain length of the PDMS used in this study was ~250 nm, the formation of a random-coiled structure can involve the conformational rearrangement of large spatial regions on the interface, compared to the local segmental substitution of charge-dipole interaction. The time required to move a molecular segment in a bulk viscous flow depends on its travel distance, and the rearrangement of such a large region will be significantly retarded by the bulk viscous flow. Therefore, it is reasonable that the time required for random-coiling can be much longer than that for the substitution of the charge-dipole bond, and that bulk viscosity becomes the rate-limiting mechanism for the entire reaction of the disappearance of layered structure.

Conclusion

The interfacial structures of 9750 mPa·s PDMS / mica interface were investigated by FM-AFM with qPlus sensor. The interfaces settled for 25 h and 29 h at room temperature after contacting showed the disordered and the layered density distributions on Δf, respectively. The approaching and retracting Δf-z curves obtained on the layered region overlapped, which suggests that the layered structure was stable or metastable. Also, an increase of $\Delta\gamma$ in excess of the hydrodynamic effect was observed near (~1-2 nm) the solid surface, which suggests the intense attraction between the solid surface and the closest liquid molecules.

Furthermore, the stabilization of the interfacial structure was further examined by separating the short-range interaction forces from the long-range interaction forces. The long-range repulsive conservative force was observed near the solid surface, which acted over a long distance from the

solid surface (about 2-3 nm) after settling for a longer time at room temperature or heating. The layered density distributions were suppressed by settling for a more extended time at room temperature or heating at 80 ℃. This finally disappeared by settling at room temperature for 142 h; however, it remained after the heating for 16 h, followed by settling at room temperature for 24 h. The temperature dependence and the activation energy of this relaxation process are close to that for bulk viscoelastic relaxation, suggesting that it is mainly rate-limited by the same mechanism as bulk viscoelastic relaxation. On the other hand, the increase of the decay length for the long-range repulsive force on the interface showed a steeper time-temperature dependence and a larger activation energy than the bulk viscoelastic relaxation, which implies they were rate-limited by the activation energy for substitution of the molecular segments interacting with the solid surface.

ASSOCIATED CONTENT

Supporting Information

Investigation on 970 mPa·s PDMS/mica interfaces prepared with and without spin-coating, and the double-exponential curves and coefficients for Δf-z curve fitting.

AUTHOR INFORMATION

Corresponding Author

Takashi Ichii

Department of Materials Science and Engineering, Kyoto University, Kyoto, 606-8501, Japan.

https://orcid.org/0000-0002-4021-8894

E-mail: ichii.takashi.2m@kyoto-u.ac.jp

Authors

Yuto Nishiwaki

Department of Materials Science and Engineering, Kyoto University, Kyoto, 606-8501, Japan.

https://orcid.org/0009-0002-9550-326X

Yuya Yamada

Department of Materials Science and Engineering, Kyoto University, Kyoto, 606-8501, Japan.

https://orcid.org/0000-0002-7652-0024

Toru Utsunomiya

Department of Materials Science and Engineering, Kyoto University, Kyoto, 606-8501, Japan.

https://orcid.org/0000-0002-0023-7812

Hiroyuki Sugimura

Department of Materials Science and Engineering, Kyoto University, Kyoto, 606-8501, Japan.

https://orcid.org/0000-0002-6415-8558

Author Contributions

Y.N. drafted the original paper. Y.N. and Y.Y. performed the AFM experiment. T.I. developed the AFM equipment and coordinated the project. Y.Y., T.I., T.U., and H.S. contributed to the interpretation of the results. All authors discussed the results and contributed to the preparation of the paper.

Notes

The authors declare no competing financial interest.

ACKNOWLEDGMENT

We thank Prof. Kuniaki Murase and Mr. Haruki Katori at Kyoto University for their help in measuring the bulk viscosity of PDMS. This work was supported by a Grant-in-Aid for Scientific Research B (JP23H01850) from Japan Society for the Promotion of Science (JSPS).

REFERENCES

(1) Ito, Y.; Shishido, S. Critical Molecular Weight for Onset of Non-Newtonian Flow and Upper Newtonian Viscosity of Polydimethylsiloxane. *J Polym Sci Part A-2 Polym Phys* **1972**, *10* (11), 2239–2248. https://doi.org/10.1002/pol.1972.180101111.

(2) Schreiber, H. P.; Bagley, E. B.; West, D. C. Viscosity/Molecular Weight Relation in Bulk Polymers-I. *Polymer (Guildf)* **1963**, *4* (C), 355–364. https://doi.org/10.1016/0032-3861(63)90042-9.

(3) Bagley, E. B.; West, D. C. Chain Entanglement and Non-Newtonian Flow. *J Appl Phys* **1958**, *29* (10), 1511–1512. https://doi.org/10.1063/1.1722979.

(4) Horn, R. G.; Israelachvili, J. N. Molecular Organization and Viscosity of a Thin Film of Molten Polymer between Two Surfaces As Probed by Force Measurements. *Macromolecules* **1988**, *21* (9), 2836–2841. https://doi.org/10.1021/ma00187a032.

(5) Yamada, S. Layering Transitions and Tribology of Molecularly Thin Films of Poly(Dimethylsiloxane). *Langmuir* **2003**, *19* (18), 7399–7405. https://doi.org/10.1021/la0345111.

(6) Evmenenko, G.; Mo, H.; Kewalramani, S.; Dutta, P. Conformational Rearrangements in Interfacial Region of Polydimethylsiloxane Melt Films. *Polymer (Guildf)* **2006**, *47* (3), 878–882. https://doi.org/10.1016/j.polymer.2005.12.010.

(7) Yu, C.; Evmenenko, G.; Kmetko, J.; Dutta, P. Effects of Shear Flow on Interfacial Ordering in Liquids: X-Ray Scattering Studies. *Langmuir* **2003**, *19* (23), 9558–9561. https://doi.org/10.1021/la0342722.

(8) Evmenenko, G.; Dugan, S. W.; Kmetko, J.; Dutta, P. Molecular Ordering in Thin Liquid Films of Polydimethylsiloxanes. *Langmuir* **2001**, *17* (13), 4021–4024. https://doi.org/10.1021/la0017734.

(9) Sun, G.; Kappl, M.; Pakula, T.; Kremer, K.; Butt, H. J. Equilibrium Interaction of Solid Surfaces across a Polymer Melt. *Langmuir* **2004**, *20* (19), 8030–8034. https://doi.org/10.1021/la049010u.

(10) Sun, G.; Butt, H.-J. Adhesion between Solid Surfaces in Polymer Melts: Bridging of Single Chains. *Macromolecules* **2004**, *37* (16), 6086–6089. https://doi.org/10.1021/ma0497714.

(11) Yamada, S. Nanotribology of Poly(Dimethylsiloxane) Melt Confined between Hydrophobic Surfaces. *Tribology Online* **2006**, *1* (2), 29–33. https://doi.org/10.2474/trol.1.29.

(12) Albrecht, T. R.; Grütter, P.; Horne, D.; Rugar, D. Frequency Modulation Detection Using High-Q Cantilevers for Enhanced Force Microscope Sensitivity. *J Appl Phys* **1991**, *69* (2), 668–673. https://doi.org/10.1063/1.347347.

(13) Fukuma, T.; Kobayashi, K.; Matsushige, K.; Yamada, H. True Atomic Resolution in Liquid by Frequency-Modulation Atomic Force Microscopy. *Appl Phys Lett* **2005**, *87* (3), 034101. https://doi.org/10.1063/1.1999856.

(14) Fukuma, T. Water Distribution at Solid/Liquid Interfaces Visualized by Frequency Modulation Atomic Force Microscopy. *Sci Technol Adv Mater* **2010**, *11* (3), 033003. https://doi.org/10.1088/1468-6996/11/3/033003.

(15) Fukui, K. I.; Utsunomiya, T.; Yokota, Y. Potential Dependent Structure of Electric Double Layer Faced to Solid Electrode Surfaces Analyzed by Electrochemical Frequency Modulation Atomic Force Microscopy. *Jpn J Appl Phys* **2017**, *56* (8). https://doi.org/10.7567/JJAP.56.08LA03.

(16) Miyata, K.; Kawagoe, Y.; Tracey, J.; Miyazawa, K.; Foster, A. S.; Fukuma, T. Variations in Atomic-Scale Step Edge Structures and Dynamics of Dissolving Calcite in Water

Revealed by High-Speed Frequency Modulation Atomic Force Microscopy. *Journal of Physical Chemistry C* **2019**, *123* (32), 19786–19793. https://doi.org/10.1021/acs.jpcc.9b05788.

(17) Hiasa, T.; Kimura, K.; Onishi, H. Hydration of Hydrophilic Thiolate Monolayers Visualized by Atomic Force Microscopy. *Physical Chemistry Chemical Physics* **2012**, *14* (23), 8419–8424. https://doi.org/10.1039/c2cp40252a.

(18) Umeda, K.; Kobayashi, K.; Minato, T.; Yamada, H. Atomic-Scale Three-Dimensional Local Solvation Structures of Ionic Liquids. *Journal of Physical Chemistry Letters* **2020**, *11* (4), 1343–1348. https://doi.org/10.1021/acs.jpclett.9b03874.

(19) Siretanu, I.; Ebeling, D.; Andersson, M. P.; Stipp, S. L. S.; Philipse, A.; Stuart, M. C.; Van Den Ende, D.; Mugele, F. Direct Observation of Ionic Structure at Solid-Liquid Interfaces: A Deep Look into the Stern Layer. *Sci Rep* **2014**, *4*, 19–21. https://doi.org/10.1038/srep04956.

(20) Hofbauer, W.; Ho, R. J.; Hairulnizam, R.; Gosvami, N. N.; O'Shea, S. J. Crystalline Structure and Squeeze-out Dissipation of Liquid Solvation Layers Observed by Small-Amplitude Dynamic AFM. *Phys Rev B* **2009**, *80*, 134104. https://doi.org/10.1103/PhysRevB.80.134104.

(21) Giessibl, F. J. The QPlus Sensor, a Powerful Core for the Atomic Force Microscope. *Review of Scientific Instruments* **2019**, *90* (1), 011101. https://doi.org/10.1063/1.5052264.

(22) Seeholzer, T.; Tarau, D.; Hollendonner, L.; Auer, A.; Rachel, R.; Grohmann, D.; Giessibl, F.; Weymouth, A. A Next-Generation QPlus-Sensor-Based AFM Setup: Resolving Archaeal S-Layer Protein Structures in Air and Liquid. *J Phys Chem B* **2023**, *127*. https://doi.org/10.1021/acs.jpcb.3c02875.

(23) Ichii, T.; Fujimura, M.; Negami, M.; Murase, K.; Sugimura, H. Frequency Modulation Atomic Force Microscopy in Ionic Liquid Using Quartz Tuning Fork Sensors. *Jpn J Appl Phys* **2012**, *51* (8 PART 4), 08KB08. https://doi.org/10.1143/JJAP.51.08KB08.

(24) Barry, A. J. Viscometric Investigation of Dimethylsiloxane Polymers. *J Appl Phys* **1946**, *17* (12), 1020–1024. https://doi.org/10.1063/1.1707670.

(25) Yamada, Y.; Ichii, T.; Utsunomiya, T.; Sugimura, H. Visualizing Polymeric Liquid/Solid Interfaces by Atomic Force Microscopy Utilizing Quartz Tuning Fork Sensors. *Jpn J Appl Phys* **2020**, *59* (SN), SN1009. https://doi.org/10.35848/1347-4065/ab84b0.

(26) Collins, E. A.; Metzger, A. P. Polyvinylchloride Melt Rheology II—the Influence of Molecular Weight on Flow Activation Energy. *Polym Eng Sci* **1970**, *10* (2), 57–65. https://doi.org/10.1002/pen.760100202.

(27) Ferry, J. D. *Viscoelastic Properties of Polymers*, 3rd ed.; John Wiley & Sons, 1980.

(28) TAMAMUSHI, R. A Note on the Activation Energy for the Viscous Flow of Aqueous Solutions. *Denki Kagaku oyobi Kogyo Butsuri Kagaku* **1986**, *54* (4), 344–346. https://doi.org/10.5796/kogyobutsurikagaku.54.344.

(29) Barlow, A. J.; Harrison, G.; Lamb, J.; Robertson, J. M. Viscoelastic Relaxation of Polydimethylsiloxane Liquids. *Proc R Soc Lond A Math Phys Sci* **1997**, *282* (1389), 228–251. https://doi.org/10.1098/rspa.1964.0229.

(30) Kirst, K. U.; Kremer, F.; Pakula, T.; Hollingshurst, J. Molecular Dynamics of Cyclic and Linear Poly(Dimethylsiloxanes). *Colloid Polym Sci* **1994**, *272* (11), 1420–1429. https://doi.org/10.1007/BF00654172.

(31) Huber, F.; Giessibl, F. J. Low Noise Current Preamplifier for QPlus Sensor Deflection Signal Detection in Atomic Force Microscopy at Room and Low Temperatures. *Review of Scientific Instruments* **2017**, *88* (7), 073702. https://doi.org/10.1063/1.4993737.

(32) Gotsmann, B.; Seidel, C.; Anczykowski, B.; Fuchs, H. Conservative and Dissipative Tip-Sample Interaction Forces Probed with Dynamic Afm. *Phys Rev B Condens Matter Mater Phys* **1999**, *60* (15), 11051–11061. https://doi.org/10.1103/PhysRevB.60.11051.

(33) Emslie, A. G.; Bonner, F. T.; Peck, L. G. Flow of a Viscous Liquid on a Rotating Disk. *J Appl Phys* **1958**, *29* (5), 858–862. https://doi.org/10.1063/1.1723300.

(34) Sides, S. W.; Curro, J.; Grest, G. S.; Stevens, M. J.; Soddemann, T.; Habenschuss, A.; Londono, J. D. Structure of Poly(Dimethylsiloxane) Melts: Theory, Simulation, and Experiment. *Macromolecules* **2002**, *35* (16), 6455–6465. https://doi.org/10.1021/ma020014k.

(35) Albouy, P. A. The Conformation of Poly(Dimethylsiloxane) in the Crystalline State. *Polymer (Guildf)* **2000**, *41* (8), 3083–3086. https://doi.org/10.1016/S0032-3861(99)00664-3.

(36) Watkins, M.; Reischl, B. A Simple Approximation for Forces Exerted on an AFM Tip in Liquid. *J Chem Phys* **2013**, *138* (15), 154703. https://doi.org/10.1063/1.4800770.

(37) Amano, K. I.; Suzuki, K.; Fukuma, T.; Takahashi, O.; Onishi, H. The Relationship between Local Liquid Density and Force Applied on a Tip of Atomic Force Microscope: A Theoretical Analysis for Simple Liquids. *Journal of Chemical Physics* **2013**, *139* (22). https://doi.org/10.1063/1.4839775.

(38) Kuo, C. J.; Lan, W. L. Gel Spinning of Synthetic Polymer Fibres. In *Advances in filament yarn spinning of textiles and polymers*; Zhang, D., Ed.; Woodhead Publishing Ltd., 2014; pp 100–112. https://doi.org/10.1533/9780857099174.2.100.

(39) Kuo, C. M. Poly(Dimethylsiloxane). In *Polymer Data Handbook*; Mark, J. E., Ed.; Oxford University Press, 1998; pp 411–435.

(40) Rouse, P. E. A Theory of the Linear Viscoelastic Properties of Dilute Solutions of Coiling Polymers. *J Chem Phys* **1953**, *21* (7), 1272–1280. https://doi.org/10.1063/1.1699180.

(41) De Gennes, P. G. Reptation of a Polymer Chain in the Presence of Fixed Obstacles. *P.G. De Gennes' Impact on Science: Soft Matter and Biophysics* **2009**, *2*, 35–42. https://doi.org/10.1142/9789812564849_0015.

(42) Jeffery, S.; Hoffmann, P. M.; Pethica, J. B.; Ramanujan, C.; Özer, H. Ö.; Oral, A. Direct Measurement of Molecular Stiffness and Damping in Confined Water Layers. *Phys Rev B Condens Matter Mater Phys* **2004**, *70* (5), 054114. https://doi.org/10.1103/PhysRevB.70.054114.

(43) Reed, P. E. *Mechanical Properties and Testing of Polymers*; Swallowe, G. M., Ed.; Polymer Science and Technology Series; Springer Netherlands: Dordrecht, 1999; Vol. 3. https://doi.org/10.1007/978-94-015-9231-4.

(44) Sun, G.; Stark, R.; Kappl, M.; Leermakers, F. A. M.; Butt, H. J. Interaction between Two Solid Surfaces across Pdms: Influence of Chain Length and End Group. *Compos Interfaces* **2005**, *12* (8–9), 805–815. https://doi.org/10.1163/156855405774984066.

(45) Sader, J. E.; Jarvis, S. P. Accurate Formulas for Interaction Force and Energy in Frequency Modulation Force Spectroscopy. *Appl Phys Lett* **2004**, *84* (10), 1801–1803. https://doi.org/10.1063/1.1667267.

(46) Kimura, K.; Ido, S.; Oyabu, N.; Kobayashi, K.; Hirata, Y.; Imai, T.; Yamada, H. Visualizing Water Molecule Distribution by Atomic Force Microscopy. *Journal of Chemical Physics* **2010**, *132* (19). https://doi.org/10.1063/1.3408289.

(47) Arrighi, V.; Higgins, J. S.; Burgess, A. N.; Floudas, G. Local Dynamics of Poly(Dimethyl Siloxane) in the Presence of Reinforcing Filler Particles. *Polymer (Guildf)* **1998**, *39* (25), 6369–6376. https://doi.org/10.1016/S0032-3861(98)00139-6.

(48) Harton, S. E.; Kumar, S. K.; Yang, H.; Koga, T.; Hicks, K.; Lee, H.; Mijovic, J.; Liu, M.; Vallery, R. S.; Gidley, D. W. Immobilized Polymer Layers on Spherical Nanoparticles. *Macromolecules* **2010**, *43* (7), 3415–3421. https://doi.org/10.1021/ma902484d.

(49) Dealy, J. M.; Wissbrun, K. F. *Melt Rheology and Its Role in Plastics Processing*; Springer Netherlands: Dordrecht, 1999; Vol. 99. https://doi.org/10.1007/978-94-009-2163-4.

(50) Shih, H.; Flory, P. J. Equation-of-State Parameters for Poly (Dimethylsiloxane). **1971**, *141* (1), 758–761.

(51) Schwarzl, F.; Staverman, A. J. Time-Temperature Dependence of Linear Viscoelastic Behavior. *J Appl Phys* **1952**, *23* (8), 838–843. https://doi.org/10.1063/1.1702316.

(52) Tobolsky, A. V. Stress Relaxation Studies of the Viscoelastic Properties of Polymers. *J Appl Phys* **1956**, *27* (7), 673–685. https://doi.org/10.1063/1.1722465.

(53) Clarson, S. J.; Dodgson, K.; Semlyen, J. A. Studies of Cyclic and Linear Poly(Dimethylsiloxanes): 19. Glass Transition Temperatures and Crystallization Behaviour. *Polymer (Guildf)* **1985**, *26* (6), 930–934. https://doi.org/10.1016/0032-3861(85)90140-5.

(54) Di Marzio, E. A.; Guttman, C. M. The Glass Temperature of Polymer Rings. *Macromolecules* **1987**, *20* (6), 1403–1407. https://doi.org/10.1021/ma00172a040.

TOC Image